

Controllable transmission spectrum via electromagnetically induced transparency with Rydberg atoms

Dexi Guo(郭德玺), Jialing Xie(谢佳凌), Chao Hang(杭超), Chengjie Zhu(朱成杰)
Citation: Chin. Phys. B.2026. 35(**8**): 084203. DOI: 10.1088/1674-1056/ae1a49
http://cpb.iphy.ac.cn; http://iopscience.iop.org/cpb

What follows is a list of articles you may be interested in

Generation of structure light in probe absorption spectrum via microwave-driven Y-type atomic system

Muhammad Saeed and Muqaddar Abbas
Chin. Phys. B, 2023, 32 (**12**): 124211. DOI: 10.1088/1674-1056/aceee7

Nonreciprocal negative refraction in a dense hot atomic medium

Hai Yi(易海), Hongjun Zhang(张红军), and Hui Sun(孙辉)
Chin. Phys. B, 2023, 32 (**4**): 044202. DOI: 10.1088/1674-1056/acae7a

Dual-function terahertz metasurface based on vanadium dioxide and graphene

Jiu-Sheng Li(李九生)† and Zhe-Wen Li(黎哲文)
Chin. Phys. B, 2022, 31 (**9**): 094201. DOI: 10.1088/1674-1056/ac5884

A low noise, high fidelity cross phase modulation in multi-level atomic medium

Liangwei Wang(王亮伟), Jia Guan(关佳), Chengjie Zhu(朱成杰), Runbing Li(李润兵), and Jing Shi(石兢)
Chin. Phys. B, 2021, 30 (**11**): 114204. DOI: 10.1088/1674-1056/ac078d

Quantum storage of single photons with unknown arrival time and pulse shapes

Yu You(由玉), Gong-Wei Lin(林功伟), Ling-Juan Feng(封玲娟), Yue-Ping Niu(钮月萍), and Shang-Qing Gong(龚尚庆)
Chin. Phys. B, 2021, 30 (**8**): 084207. DOI: 10.1088/1674-1056/abfbd3

SPECIAL TOPIC — Quantum frontiers with Rydberg atoms

Controllable transmission spectrum via electromagnetically induced transparency with Rydberg atoms

Dexi Guo(郭德玺)[1], Jialing Xie(谢佳凌)[1], Chao Hang(杭超)[2,3,4,†], and Chengjie Zhu(朱成杰)[1,‡]

[1] *School of Physical Science and Technology, Soochow University, Suzhou* 215006, *China*
[2] *Institute of Quantum Science and Precision Measurement, East China Normal University, Shanghai* 200241, *China*
[3] *NYU-ECNU Institute of Physics, New York University Shanghai, Shanghai* 200062, *China*
[4] *Collaborative Innovation Center of Extreme Optics, Shanxi University, Taiyuan* 030006, *China*

(Received 10 September 2025; revised manuscript received 20 October 2025; accepted manuscript online 3 November 2025)

Controllable transmission spectrum is highly desirable in optics. Here we investigate the transmission spectrum and its control using cascaded electromagnetically induced transparency (EIT) with Rydberg atoms. We show that the transmission spectrum of the probe field can exhibit one or no EIT transparency window if the atomic vapor contains mainly the Rydberg-blockaded three-level atoms or Rydberg four-level atoms. Moreover, the transmission spectrum can be actively controlled by tuning the ratio between the control and driving laser fields, rendering various applications in optical processing, such as optical absorbers.

Keywords: electromagnetically induced transparency and absorption, nonlinear optics, Rydberg states

PACS: 42.50.Gy, 42.65.–k, 32.80.Ee

DOI: 10.1088/1674-1056/ae1a49 **CSTR:** 32038.14.CPB.ae1a49

1. Introduction

The transmission spectrum is obtained by measuring the relative intensity of light at the output port and the input port. It describes how much light can be transmitted to the other side of the waveguide at different wavelengths.[1] In conventional solid materials such as optical fibers and waveguides, the transmission spectrum is difficult to control in an active manner. However, a system with a controllable transmission spectrum is highly useful for many applications in the fields of optical information processing and transmission.[2]

On the other hand, optical materials with *nonlocal* nonlinearities are of great interest due to their intriguing physics and practical applications.[3] Optical nonlocality means that the refractive index at a particular location is determined by the light intensity over an extended region of the optical medium. It can arise through a variety of physical mechanisms such as atomic diffusion,[4] photorefractive effect,[5,6] interactions in liquid crystals,[7] thermal self-action,[8,9] electron transport in plasma,[10] dipole-dipole interactions in ultracold quantum gases,[11] Rydberg atomic gases,[12] etc.

Rydberg atomic gases working under the condition of electromagnetically induced transparency (EIT)[13–15] possess many unique properties, and hence have attracted tremendous attention in recent years. Firstly, the optical absorption due to the resonance between optical fields and atoms can be greatly suppressed via EIT, a quantum destructive interference effect induced by a control laser field. Secondly, Rydberg-EIT systems can map the strong and long-range interaction [i.e., the Rydberg–Rydberg interaction (RRI)] between atoms in Rydberg states into the strong and long-range interaction between photons,[16] resulting in a giant and nonlocal optical Kerr nonlinearity. Thirdly, such Rydberg-EIT systems are configurable and controllable in an active way due to the existence of many tunable parameters, such as atomic levels, detuning, and laser intensities. Based on these striking features, Rydberg-EIT systems have become an excellent platform for the research of quantum and nonlinear optics in strongly interacting atomic ensembles,[16–24] and have promising applications in many fields such as high-precision measurement and quantum information processing.[25–28]

In this work, we investigate the transmission spectrum and its control using cascaded EIT with Rydberg atoms. We show that the transmission spectrum of the probe field can exhibit one or two EIT transparency windows if the atomic vapor is dominated by Rydberg-blockaded three-level atoms or Rydberg four-level atoms, respectively. Moreover, the transmission spectrum can be actively controlled by the Rydberg blockade radius, which further depends on the ratio between the control and driving laser fields in the system. The findings in this work render a variety of applications in optical processing, such as the design of optical absorbers.

[†]Corresponding author. E-mail: chang@phy.ecnu.edu.cn
[‡]Corresponding author. E-mail: cjzhu@suda.edu.cn

© 2026 Chinese Physical Society and IOP Publishing Ltd. All rights, including for text and data mining, AI training, and similar technologies, are reserved.

2. Model

We start by considering a lifetime-broadened four-level atomic system with a cascaded configuration,[29,30] shown in Fig. 1(a). The electric field acting on the atomic system reads $\boldsymbol{E}=\boldsymbol{E}_{\rm p}+\boldsymbol{E}_{\rm d}+\boldsymbol{E}_{\rm c}$, with $\boldsymbol{E}_{\alpha}=\boldsymbol{e}_{\alpha}\mathcal{E}_{\alpha}\exp[{\rm i}(\boldsymbol{k}_{\alpha}\cdot\boldsymbol{r}-\omega_{\alpha}t)]+$ h.c. ($\boldsymbol{e}_{\alpha}$ are unit polarization vectors, $\mathcal{E}_{\alpha}$ are field amplitudes). Here, a weak, spatially focused probe laser field $\boldsymbol{E}_{\rm p}$ (with wavenumber $k_{\rm p}=\omega_{\rm p}/c$, angular frequency $\omega_{\rm p}$, and Rabi frequency $\Omega_{\rm p}$) couples the ground state $|1\rangle$ to the intermediate state $|2\rangle$; a strong driving laser field $\boldsymbol{E}_{\rm d}$ (with wavenumber $k_{\rm d}=\omega_{\rm d}/c$, angular frequency $\omega_{\rm d}$, and Rabi frequency $\Omega_{\rm d}$) couples the intermediate state $|2\rangle$ to the excited state $|3\rangle$. States $|1\rangle$, $|2\rangle$, and $|3\rangle$, together with the probe and driving fields, constitute a standard cascaded Ξ-type EIT configuration. The Ξ-type EIT is, however, dressed by a high-lying Rydberg state $|4\rangle$, with a large principal quantum number n. The Rydberg state $|4\rangle$ is coupled to $|3\rangle$ through a control laser field $\boldsymbol{E}_{\rm c}$ (with wavenumber $k_{\rm c}=\omega_{\rm c}/c$, angular frequency $\omega_{\rm c}$, and Rabi frequency $\Omega_{\rm c}$). Here, $\Delta_{\rm p}=\omega_{\rm p}-(\omega_2-\omega_1)$ is the one-photon detuning, $\Delta_{\rm d}=\omega_{\rm p}+\omega_{\rm d}-(\omega_3-\omega_1)$ is the two-photon detuning, and $\Delta_{\rm c}=\omega_{\rm p}+\omega_{\rm d}+\omega_{\rm c}-(\omega_4-\omega_1)$ is the three-photon detuning, with ω_j the eigenfrequency of the level $|j\rangle$; Γ_{12}, Γ_{23}, and Γ_{34} are respectively the spontaneous-emission decay rates from $|2\rangle$ to $|1\rangle$, $|3\rangle$ to $|2\rangle$, and $|4\rangle$ to $|3\rangle$. This yields the N-atom Hamiltonian

$$\hat{H}=\sum_{\alpha}^{N}\hat{H}_{\alpha}+\sum_{\alpha\neq\beta}^{N}\frac{\hbar V(\boldsymbol{r}_{\alpha}-\boldsymbol{r}_{\beta})}{2}\hat{\sigma}_{44}^{\alpha}\hat{\sigma}_{44}^{\beta},\tag{1}$$

where $\hat{H}_{\alpha}/\hbar=\Delta_{\rm p}\hat{\sigma}_{22}^{\alpha}+\Delta_{\rm d}\hat{\sigma}_{33}^{\alpha}+\Delta_{\rm c}\hat{\sigma}_{44}^{\alpha}+\Omega_{\rm p}\hat{\sigma}_{21}^{\alpha}+\Omega_{\rm c}\hat{\sigma}_{32}^{\alpha}+\Omega_{\rm d}\hat{\sigma}_{43}^{\alpha}+$H.c. is the αth atom Hamiltonian with $\sigma_{ij}^{\alpha}=|i^{\alpha}\rangle\langle j^{\alpha}|$ $(i,j=1-4)$. Here, the Rabi frequencies of the probe, driving, and control fields are respectively $\Omega_{\rm p}=(\boldsymbol{e}_{\rm p}\cdot\boldsymbol{p}_{21})\mathcal{E}_{\rm p}/\hbar$, $\Omega_{\rm d}=(\boldsymbol{e}_{\rm d}\cdot\boldsymbol{p}_{32})\mathcal{E}_{\rm d}/\hbar$, and $\Omega_{\rm c}=(\boldsymbol{e}_{\rm c}\cdot\boldsymbol{p}_{43})\mathcal{E}_{\rm c}/\hbar$, with $\boldsymbol{p}_{ij}$ the electric dipole matrix elements associated with the transition $|i\rangle\leftrightarrow|j\rangle$.

Under the electric-dipole and rotating-wave approximations, and applying the continuous density approximation, the motion of the density matrix elements, $\rho_{jl}\equiv\langle\hat{\sigma}_{jl}\rangle$, is described by the optical Bloch equations

$${\rm i}\frac{\partial}{\partial t}\rho_{11}-{\rm i}\Gamma_{12}\rho_{22}-\Omega_{\rm p}\rho_{12}+\Omega_{\rm p}^{*}\rho_{21}=0,\tag{2a}$$

$${\rm i}\left(\frac{\partial}{\partial t}+\Gamma_{12}\right)\rho_{22}-{\rm i}\Gamma_{23}\rho_{33}-\Omega_{\rm d}\rho_{23}+\Omega_{\rm d}^{*}\rho_{32}+\Omega_{\rm p}\rho_{12}-\Omega_{\rm p}^{*}\rho_{21}=0,\tag{2b}$$

$${\rm i}\left(\frac{\partial}{\partial t}+\Gamma_{23}\right)\rho_{33}-{\rm i}\Gamma_{34}\rho_{44}+\Omega_{\rm d}\rho_{23}-\Omega_{\rm d}^{*}\rho_{32}-\Omega_{\rm c}\rho_{34}+\Omega_{\rm c}^{*}\rho_{43}=0,\tag{2c}$$

$${\rm i}\frac{\partial}{\partial t}\rho_{44}+{\rm i}\Gamma_{34}\rho_{44}+\Omega_{\rm c}\rho_{34}-\Omega_{\rm c}^{*}\rho_{43}=0,\tag{2d}$$

for diagonal matrix elements and

$$\left({\rm i}\frac{\partial}{\partial t}+d_{21}\right)\rho_{21}+\Omega_{\rm p}(\rho_{11}-\rho_{22})+\Omega_{\rm d}^{*}\rho_{31}=0,\tag{3a}$$

$$\left({\rm i}\frac{\partial}{\partial t}+d_{31}\right)\rho_{31}-\Omega_{\rm p}\rho_{32}+\Omega_{\rm d}\rho_{21}+\Omega_{\rm c}^{*}\rho_{41}=0,\tag{3b}$$

$$\left({\rm i}\frac{\partial}{\partial t}+d_{41}\right)\rho_{41}-\Omega_{\rm p}\rho_{42}+\Omega_{\rm c}\rho_{31}-\mathcal{N}_{\alpha}\int{\rm d}^{3}\boldsymbol{r}'V(\boldsymbol{r}'-\boldsymbol{r})\rho_{44,41}(\boldsymbol{r}',\boldsymbol{r},t)=0,\tag{3c}$$

$$\left({\rm i}\frac{\partial}{\partial t}+d_{32}\right)\rho_{32}-\Omega_{\rm p}^{*}\rho_{31}+\Omega_{\rm d}(\rho_{22}-\rho_{33})+\Omega_{\rm c}^{*}\rho_{42}=0,\tag{3d}$$

$$\left({\rm i}\frac{\partial}{\partial t}+d_{42}\right)\rho_{42}-\Omega_{\rm p}^{*}\rho_{41}-\Omega_{\rm d}\rho_{43}+\Omega_{\rm c}\rho_{32}-\mathcal{N}_{\alpha}\int{\rm d}^{3}\boldsymbol{r}'V(\boldsymbol{r}'-\boldsymbol{r})\rho_{44,42}(\boldsymbol{r}',\boldsymbol{r},t)=0,\tag{3e}$$

$$\left({\rm i}\frac{\partial}{\partial t}+d_{43}\right)\rho_{43}+\Omega_{\rm c}(\rho_{33}-\rho_{44})-\Omega_{\rm d}^{*}\rho_{42}-\mathcal{N}_{\alpha}\int{\rm d}^{3}\boldsymbol{r}'V(\boldsymbol{r}'-\boldsymbol{r})\rho_{44,43}(\boldsymbol{r}',\boldsymbol{r},t)=0,\tag{3f}$$

for non-diagonal matrix elements. Here, $d_{21}=\Delta_{\rm p}+{\rm i}\gamma_{12}$, $d_{31}=\Delta_{\rm d}+{\rm i}\gamma_{13}$, $d_{41}=\Delta_{\rm c}+{\rm i}\gamma_{14}$, $d_{32}=\Delta_{\rm d}-\Delta_{\rm p}+{\rm i}\gamma_{23}$, $d_{42}=\Delta_{\rm c}-\Delta_{\rm p}+{\rm i}\gamma_{24}$, and $d_{43}=\Delta_{\rm c}-\Delta_{\rm d}+{\rm i}\gamma_{34}$; the decay rate $\gamma_{ij}=(\Gamma_i+\Gamma_j)/2+\gamma_{ij}^{\rm col}$, where $\Gamma_j=\sum_{i<j}\Gamma_{ij}$, with Γ_{ij} the spontaneous emission decay rate, and $\gamma_{ij}^{\rm col}$ the dephasing rate from $|j\rangle$ to $|i\rangle$. The last terms in Eqs. (3c), (3e), and (3f) are contributions from the interatomic interaction, where $\mathcal{N}_{\alpha}$ is the density of the atomic gas. The interaction between the Rydberg atom at position $\boldsymbol{r}$ and the one at position $\boldsymbol{r}'$ is described by the long-range potential $\hbar V(\boldsymbol{r}'-\boldsymbol{r})$, where $V(\boldsymbol{r}'-\boldsymbol{r})=C_6/|\boldsymbol{r}'-\boldsymbol{r}|^6$, with C_6 the dispersion parameter. Here, $\rho_{ij,kl}(\boldsymbol{r}',\boldsymbol{r},t)=\langle\sigma_{ij}(\boldsymbol{r}',t)\sigma_{kl}(\boldsymbol{r},t)\rangle$ is the two-body correlation.

The wave equation of the probe field is described by the Maxwell equation, which under the slowly varying amplitude approximation reads

$${\rm i}\left(\frac{\partial}{\partial z}+\frac{1}{c}\frac{\partial}{\partial t}\right)\Omega_{\rm p}+\frac{k_{\rm p}}{2}\chi_{\rm p}\Omega_{\rm p}=0,\tag{4}$$

where $\chi_{\rm p}=\mathcal{N}_{\alpha}(\boldsymbol{e}_{\rm p}\cdot\boldsymbol{p}_{12})^2\rho_{21}/(\varepsilon_0\hbar\Omega_{\rm p})$ is the probe-field susceptibility. Note that for convenience and without loss of generality, the propagation direction of the probe field is assumed to be along the z direction, i.e. $\boldsymbol{k}_{\rm p}=(0,0,k_{\rm p})$. To suppress the leading-order Doppler effect, we choose $\boldsymbol{k}_{\rm d}=(0,0,-k_{\rm d})$ and $\boldsymbol{k}_{\rm c}=(0,0,k_{\rm c})$; in addition, since we are interested in a stationary state of the system, the time derivatives in the Maxwell–Bloch Eqs. (3) and (4) can be neglected (i.e. $\partial/\partial t=0$), which is valid if the probe field has a sufficiently long duration.

We assume that atoms are initially prepared to occupy only the ground state $|1\rangle$. Since the probe field is weak, the population in atomic levels does not change significantly when

the probe field is applied to the system, and hence a standard perturbation method can be employed to solve the Maxwell–Bloch Eqs. (3) and (4) beyond the adiabatic approximation. Using the smallness of the amplitude of the probe field relative to that of the driving field, i.e. $|\Omega_{\rm p}/\Omega_{\rm c}| \ll 1$, we can employ the expansion $\rho_{jl} = \sum_{m=0}^{\infty} \rho_{jl}^{(m)}$, where $\rho_{jl}^{(m)}$ is of order $|\Omega_{\rm p}/\Omega_{\rm c}|^m$. Substituting the expansions into the Bloch equation (3) without taking into account time derivatives, Eq. (3) at the leading order is solved as $\rho_{11}^{(0)} = 1$ with the other density matrix elements being zero.

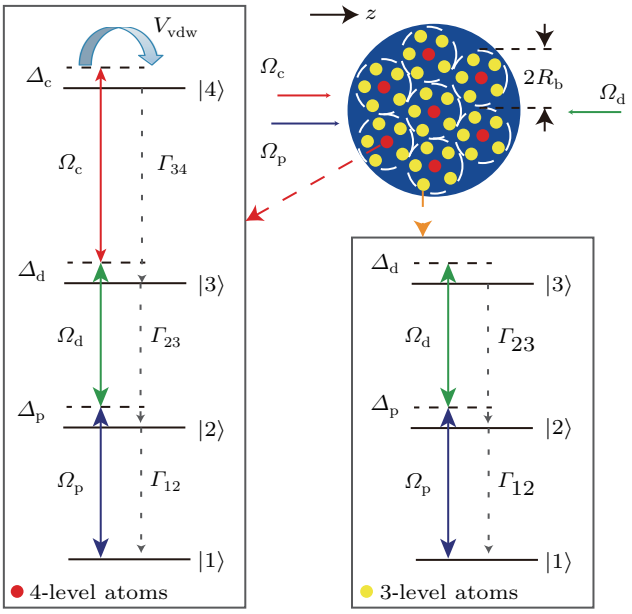


Fig. 1. Level diagram and excitation scheme of the cascaded Rydberg-EIT system. For Rydberg-blockaded atoms, states $|1\rangle$, $|2\rangle$, and $|3\rangle$ constitute a standard three-level Ξ-type EIT configuration, where the probe field (with Rabi frequency $\Omega_{\rm p}$) couples the transition $|1\rangle \leftrightarrow |2\rangle$, and the driving field (with Rabi frequency $\Omega_{\rm d}$) couples the transition $|2\rangle \leftrightarrow |3\rangle$. For Rydberg atoms, the Ξ-type EIT is further dressed by a high-lying Rydberg state $|4\rangle$, coupled to the state $|3\rangle$ through a control field (with Rabi frequency $\Omega_{\rm c}$). Δ_α ($\alpha = {\rm p, d, c}$) are detunings and Γ_{jl} is the spontaneous-emission decay rate from $|l\rangle$ to $|j\rangle$. The interaction between two Rydberg atoms is described by the van der Waals potential $V_{\rm vdw} \equiv \hbar V(\boldsymbol{r}' - \boldsymbol{r})$, with $V(\boldsymbol{r}' - \boldsymbol{r}) = C_6/|\boldsymbol{r}' - \boldsymbol{r}|^6$. $R_{\rm b}$ is the Rydberg blockade radius.

At the first order, by gathering the terms of order $|\Omega_{\rm p}/\Omega_{\rm c}|$, only a subset of three equations describes the essential dynamics. In the frequency domain, these equations describing the linear excitation of the present system are given as

$$\begin{pmatrix} \omega + d_{21} & \Omega_{\rm d}^* & 0 \\ \Omega_{\rm d} & \omega + d_{31} & \Omega_{\rm c}^* \\ 0 & \Omega_{\rm c} & \omega + d_{41} - \delta_{41} \end{pmatrix} \begin{pmatrix} \rho_{21}^{(1)} \\ \rho_{31}^{(1)} \\ \rho_{41}^{(1)} \end{pmatrix} = \begin{pmatrix} -\Omega_{\rm p} \\ 0 \\ 0 \end{pmatrix}, \tag{5}$$

leading to the solution

$$\rho_{21}^{(1)} = \frac{(\omega + d_{31})(\omega + d_{41} - \delta_{41}) - |\Omega_{\rm c}|^2}{D(\omega)} \Omega_{\rm p}, \tag{6a}$$

$$\rho_{31}^{(1)} = -\frac{(\omega + d_{41} - \delta_{41})\Omega_{\rm d}}{D(\omega)} \Omega_{\rm p}, \tag{6b}$$

$$\rho_{41}^{(1)} = \frac{\Omega_{\rm d}\Omega_{\rm c}}{D(\omega)} \Omega_{\rm p}, \tag{6c}$$

$$\rho_{jj}^{(1)} = \rho_{32}^{(1)} = \rho_{42}^{(1)} = \rho_{43}^{(1)} = 0, \quad (j = 1, 2, 3, 4), \tag{6d}$$

with $D(\omega) = |\Omega_{\rm d}|^2(\omega + d_{41}) + |\Omega_{\rm c}|^2(\omega + d_{21}) - (\omega + d_{21})(\omega + d_{31})(\omega + d_{41} - \delta_{41})$. (The frequency of the probe field is thus given by $\omega_{\rm p} + \omega$, i.e., ω stands for a small deviation from the center frequency of the probe field $\omega_{\rm p}$.) For obtaining Eq. (5), we have used the mean-field approximation, i.e., $\rho_{44,41}^{(3)} \approx \rho_{44}^{(2)}\rho_{41}^{(1)} \approx \rho_{41}^{(1)}\rho_{14}^{(1)}\rho_{41}^{(1)} = \left|\rho_{41}^{(1)}\right|^2 \rho_{41}^{(1)}$, which is only valid for a dilute atomic gas with negligible dephasing. A more rigorous approach for calculating $\rho_{44}^{(2)}$ can be carried out by using the second-order equations.[21]

The detuning δ_{41} is induced by the RRI, which can be solved by the integral

$$\begin{aligned} \delta_{41} &= \mathcal{N}_\alpha \left(\int_0^{R_{\rm b}} \frac{C_6}{R_{\rm b}^6} \rho_{44}^{(2)} 4\pi R^2 {\rm d}R + \int_{R_{\rm b}}^{\infty} \frac{C_6}{R^6} \rho_{44}^{(2)} 4\pi R^2 {\rm d}R \right) \\ &= \mathcal{N}_\alpha \frac{8\pi C_6}{3R_{\rm b}^3} |\rho_{41}^{(1)}|^2 \\ &\approx \mathcal{N}_\alpha \frac{8\pi C_6}{3R_{\rm b}^3} \frac{|\Omega_{\rm d}\Omega_{\rm c}\Omega_{\rm p}|^2}{||\Omega_{\rm d}|^2 d_{41} + |\Omega_{\rm c}|^2 d_{21} - d_{21}d_{31}(d_{41} - \delta_{41})|^2}. \end{aligned} \tag{7}$$

Here, the Rydberg blockade radius $R_{\rm b}$ is estimated by $R_{\rm b} = (|C_6/\delta_{\rm EIT}|)^{1/6}$, where $\delta_{\rm EIT}$ is the linewidth of the EIT transmission spectrum (i.e., the width of the EIT transparency window), calculated by $\delta_{\rm EIT} = |\Omega_{\rm d}|^2|\Omega_{\rm c}|^2/(|d_{31}|^2|d_{41}|)$. Since δ_{41} should be of order one [i.e., $\delta_{41} \sim \mathcal{O}(1)$], it requires that $\mathcal{N}_\alpha C_6/R_{\rm b}^3 \sim |\Omega_{\rm p}/\Omega_{\rm c}|^{-2}$ and hence $|\Omega_{\rm p}/\Omega_{\rm c}| \sim R_{\rm b}^{3/2}/(\mathcal{N}_\alpha C_6)^{1/2}$.

To evaluate the role of RRI in the change in the transmission, we postulate that any atom has a probability of being a Rydberg four-level atom, driven by the driving and control laser fields, and a Rydberg-blockaded three-level atom, driven only by the driving laser field. Accordingly, the susceptibility of the probe field can be expressed as[31]

$$\chi_{\rm p} = \chi_{\rm 4L} + \chi_{\rm 3L}, \tag{8}$$

where $\chi_{\rm 4L}$ is the susceptibility for Rydberg four-level atoms and $\chi_{\rm 3L}$ is the susceptibility for Rydberg-blockaded three-level atoms. To first order, the susceptibility of the Rydberg four-level atoms reads

$$\chi_{\rm 4L} = \frac{\mathcal{N}_{\rm 4L}|\boldsymbol{e}_{\rm p} \cdot \boldsymbol{p}_{13}|^2}{\varepsilon_0 \hbar} \frac{(\omega + d_{31})(\omega + d_{41} - \delta_{41}) - |\Omega_{\rm c}|^2}{D(\omega)}, \tag{9}$$

where δ_{41} is included in the term $D(\omega)$ and can be computed by Eq. (7); the susceptibility of the Rydberg-blockaded three-level atoms is

$$\chi_{\rm 3L} = \frac{\mathcal{N}_{\rm 3L}|\boldsymbol{e}_{\rm p} \cdot \boldsymbol{p}_{13}|^2}{\varepsilon_0 \hbar} \frac{\omega + d_{31}}{|\Omega_{\rm d}|^2 - (\omega + d_{21})(\omega + d_{31})}. \tag{10}$$

Here, $\mathcal{N}_{4L}$ and $\mathcal{N}_{3L}$ are respectively the densities of Rydberg and Rydberg-blockaded atoms, with the total atomic density $\mathcal{N}_\alpha = \mathcal{N}_{4L} + \mathcal{N}_{3L}$.

Since only one atom can be excited to the Rydberg state in the sphere with radius R_b, if $3/(4\pi R_b^3) < \mathcal{N}_\alpha$, i.e. $R_b > \sqrt[3]{3/(4\pi\mathcal{N}_\alpha)}$ (for a large blockade radius), the densities of Rydberg and Rydberg-blockaded atoms are respectively $\mathcal{N}_{4L} = 3/(4\pi R_b^3)$ and $\mathcal{N}_{3L} = \mathcal{N}_\alpha - \mathcal{N}_{4L}$. On the other hand, if $3/(4\pi R_b^3) \geq \mathcal{N}_\alpha$, i.e. $R_b \leq \sqrt[3]{3/(4\pi\mathcal{N}_\alpha)}$ (for a small blockade radius), one has $\mathcal{N}_{4L} = \mathcal{N}_\alpha$ and $\mathcal{N}_{3L} = 0$.

The transmission spectrum of the probe field in the system is determined by the imaginary part of χ_p (i.e., $\mathrm{Im}(\chi_p)$). According to the Beer–Lambert law,[32] the transmission is given by

$$T_p = \mathrm{e}^{-k_p \mathrm{Im}(\chi_p) L}, \tag{11}$$

where L is the length of the medium. Therefore, the transmission spectrum can be fully manipulated by tuning the Rydberg blockade radius through changes in the laser field intensities, as shown below.

3. Controllable transmission spectrum of the Rydberg-EIT system

To have a better illustration of the controllability of the transmission spectrum, we choose a cold gas of ^{133}Cs atoms as a realistic candidate physical system that can be described by the theoretical model described above.[29,30] The assigned atomic levels are $|1\rangle = |6S_{1/2}\rangle$, $|2\rangle = |6P_{3/2}\rangle$, $|3\rangle = |7S_{1/2}\rangle$, and $|4\rangle = |30P_{3/2}\rangle$. The spontaneous decay rates are $\Gamma_2 \approx 2\pi \times 5.3$ MHz, $\Gamma_3 \approx 2\pi \times 3.3$ MHz, and $\Gamma_4 \approx 2\pi \times 0.01$ MHz, respectively. The wavelengths of the probe, driving, and control fields are respectively $\lambda_p = 852$ nm, $\lambda_d = 1470$ nm, and $\lambda_c = 786$ nm, and all detunings are assumed to be zero, i.e. $\Delta_p = \Delta_d = \Delta_c = 0$. The Rabi frequencies of the probe and driving fields are respectively $\Omega_d = 2\pi \times 5$ MHz and $\Omega_p = 2\pi \times 50$ kHz, the dispersion parameter $C_6 \approx -0.5$ GHz $\cdot$ μm^6,[30] and the total density of the atomic gas is $\mathcal{N}_a = 5 \times 10^{12}$ cm^{-3}.

Now, we discuss the transmission spectrum of the probe field for different values of the control field with the driving field fixed. Firstly, we choose the Rabi frequency of the control field to be much weaker than the driving field, say $\Omega_c = 2\pi \times 0.5$ MHz (i.e., $\Omega_c/\Omega_d = 0.1$). With the given parameters, the blockade radius is $R_b \approx 0.8$ μm, the RRI-induced frequency shift is $\delta_{41} \approx -2.53 \times 10^{12}$ s^{-1}, and the densities of four- and three-level atoms are respectively given as $\mathcal{N}_{4L} \approx 5.7 \times 10^{11}$ cm^{-3} and $\mathcal{N}_{3L} \approx 4.4 \times 10^{12}$ cm^{-3}. Since $\mathcal{N}_{4L}/\mathcal{N}_{3L} \approx 0.13 \ll 1$, the atomic gas is dominated by Rydberg-blockaded three-level atoms. In Figs. 2(a1), 2(a2), and 2(a3), we show the imaginary part of the susceptibility as a function of ω. Panels (a1), (a2), and (a3) of Fig. 2 show $\mathrm{Im}(\chi_{4L})$, $\mathrm{Im}(\chi_{3L})$, and $\mathrm{Im}(\chi_p) = \chi_{4L} + \chi_{3L}$, respectively. Obviously, $\mathrm{Im}(\chi_{3L})$ has a local minimum at $\omega = 0$ (see Fig. 2(a2)), corresponding to the EIT transparency window, which, however, disappears for $\mathrm{Im}(\chi_{4L})$ (see Fig. 2(a1)). This is because the EIT condition in Rydberg-blockaded three-level atoms is broken in Rydberg four-level atoms due to the presence of an additional laser field (i.e., the control field) and an additional level (i.e., $|4\rangle$). As a result, $\mathrm{Im}(\chi_p)$ shows only one EIT transparency window since nearly all atoms are Rydberg-blockaded (i.e., three-level atoms).

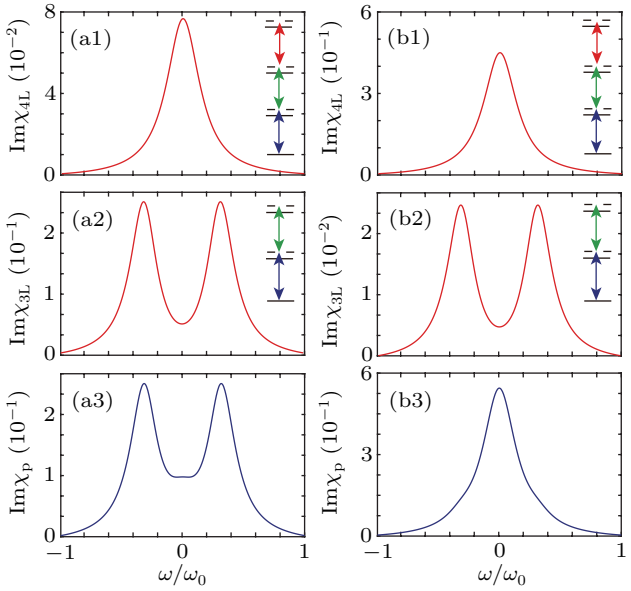


Fig. 2. The absorption of the probe field as a function of ω/ω_0 (with $\omega_0 = 1.0 \times 10^8$ s^{-1}) for $\Omega_c = 2\pi \times 0.5$ MHz ($\Omega_c/\Omega_d = 0.1$), as shown in panels (a1)–(a3), and $\Omega_c = 2\pi \times 4$ MHz ($\Omega_c/\Omega_d \approx 0.8$), as shown in panels (b1)–(b3). The upper, middle, and lower rows show $\mathrm{Im}(\chi_{4L})$, $\mathrm{Im}(\chi_{3L})$, and $\mathrm{Im}(\chi_p) = \mathrm{Im}(\chi_{4L}) + \mathrm{Im}(\chi_{3L})$, respectively.

Next, we consider the strength of the control field to be comparable to that of the driving field. To be specific, we take $\Omega_c = 2\pi \times 4$ MHz, and hence $\Omega_c/\Omega_d \approx 0.8$. With the given parameters, the blockade radius is $R_b \approx 0.4$ μm, the RRI-induced frequency shift is $\delta_{41} \approx -4.36 \times 10^{12}$ s^{-1}, and the densities of four- and three-level atoms are respectively given as $\mathcal{N}_{4L} \approx 4.6 \times 10^{12}$ cm^{-3} and $\mathcal{N}_{3L} \approx 4.1 \times 10^{11}$ cm^{-3}. Since $\mathcal{N}_{4L}/\mathcal{N}_{3L} \approx 11 \gg 1$, the atomic gas is dominated by Rydberg four-level atoms. Panels (b1), (b2), and (b3) of Fig. 2 show the same quantities as those in Figs. 2(a1), 2(a2), and 2(a3), respectively, but for a large value of Ω_c/Ω_d. It is clear that $\mathrm{Im}(\chi_p)$ shows no EIT transparency window since nearly all atoms are Rydberg four-level atoms.

To elucidate the physical process by which the control laser field Ω_c affects the Rydberg blockade radius R_b, we write R_b in the form

$$R_b^6 = \frac{|C_6|}{\delta_{EIT}} = |C_6| \frac{|d_{31}|^2 |d_{41}|}{|\Omega_c|^2 |\Omega_d|^2}. \tag{12}$$

Apparently, if Ω_d is fixed, R_b decreases rapidly as Ω_c increases. As a result, the variation of R_b changes the atomic

densities $\mathcal{N}_{4L}$ and $\mathcal{N}_{3L}$ simultaneously, which further alters χ_{4L} and χ_{3L} and hence alters $\chi_p = \chi_{4L} + \chi_{3L}$.

From the above result, the transmission spectrum T_p of the probe field can be actively controlled by changing Ω_c when Ω_d is kept constant. Figure 3(a) shows T_p, defined by Eq. (11), as a function of Ω_c/Ω_d by taking $\Omega_d = 2\pi \times 5$ MHz and $L = 1$ μm. Other parameters are the same as those used in Fig. 2. In Fig. 3(a), we see that T_p decreases rapidly with increasing Ω_c/Ω_d as $\mathrm{Im}(\chi_p)$ at $\omega = 0$ increases rapidly with increasing Ω_c/Ω_d. Particularly, we have $T_p \approx 0.43$ at $\Omega_c/\Omega_d = 0.1$ and $T_p \approx 0.04$ at $\Omega_c/\Omega_d = 0.8$. Moreover, we illustrate R_b as a function of Ω_c/Ω_d according to Eq. (12), as shown in the inset of Fig. 3(a), which is monotonically decreasing. Figure 3(b) and Fig. 3(c) show the propagation of the probe field intensity $|\Omega_p|^2$ at $\Omega_c/\Omega_d = 0.1$ and $\Omega_c/\Omega_d = 0.8$, respectively. Clearly, the probe field attenuates slightly in Fig. 3(b) but significantly in Fig. 3(c). The result in Fig. 3 indicates that the present system can be used for designing an optical absorber.

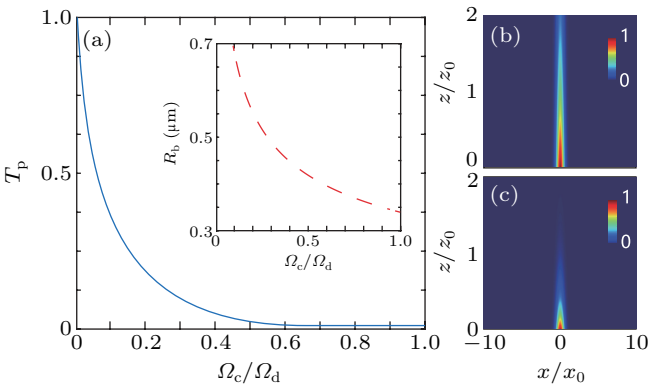


Fig. 3. (a) The transmission spectrum of the probe field T_p as a function of Ω_c/Ω_d by taking $\Omega_d = 2\pi \times 5$ MHz and $L = 1$ μm. Other parameters are the same as those used in Fig. 2. Inset: R_b as a function of Ω_c/Ω_d. (b) and (c) The probe field intensity $|\Omega_p|^2$ as a function of x/x_0 and z/z_0 (with $x_0 = z_0 = 1$ μm) for $\Omega_c/\Omega_d = 0.1$ and $\Omega_c/\Omega_d = 0.8$, respectively.

4. Conclusion

Eventually, we briefly discuss the Doppler effect due to the atoms' thermal motion. When the atoms move with velocity V, the one- and two-photon detunings for the Rydberg-blockaded three-level atoms should be replaced with $\Delta_p \to \omega_p - \omega_{21} + k_{pz}V_z$ and $\Delta_d \to (\omega_p + \omega_d) - \omega_{31} + (k_{pz} - k_{dz})V_z$ (we have assumed that the probe and driving laser fields propagate in opposite directions, as suggested in Fig. 1; the subscript "z" denotes the z-component of the corresponding quantities). The V_z-dependent terms obtained are then averaged over a given thermal velocity distribution $f(V_z)$. Then, the velocity-dependent effect in the two-photon detuning Δ_d in the counter-propagating case is much smaller than that in the co-propagating case. Consequently, the velocity-dependent effect or the Doppler effect in Δ_d can usually be neglected compared with that in the one-photon detuning if we choose the laser fields to propagate in opposite directions. Additionally, such an effect of the three-photon detuning $\Delta_c \to (\omega_p + \omega_d + \omega_c) - \omega_{41} + (k_{pz} - k_{dz} + k_{cz})V_z$ can also be suppressed.

In conclusion, we have investigated the transmission spectrum and its control through the use of cascaded EIT with Rydberg atoms. We show that the transmission spectrum of the probe field can exhibit one or two EIT transparency windows if the atomic vapor is dominated by Rydberg-blockaded three-level atoms or Rydberg four-level atoms, respectively. Moreover, the transmission spectrum can be actively controlled by tuning the ratio between the control and driving laser fields, rendering important applications in the field of optical processing such as the design of optical absorbers.

Acknowledgments

Project supported by the National Natural Science Foundation of China (Grant No. U25D9005 and 12374334), Gusu Leading Talent Plan (Grant No. ZXL2022489), National Natural Science Foundation of China (Grant No. 12374303), and Shanghai Municipal Science and Technology Major Project (Grant No. 2019SHZDZX01).

References

[1] Born M and Wolf E 2019 *Principles of Optics* (Cambridge: Cambridge University Press)
[2] Chen L T, Qin L G, Tian L J, Huang J H, Zhou N R and Gong S Q 2024 *Chin. Phys. B* **33** 064204
[3] Malomed B A 2022 *Symmetry* **14** 1565
[4] Suter D and Blasberg T 1993 *Phys. Rev. A* **48** 4583
[5] Segev M, Crosignani B, Yariv A and Fischer B 1992 *Phys. Rev. Lett.* **68** 923
[6] Królikowski W, Saffman M, Luther-Davies B and Denz C 1998 *Phys. Rev. Lett.* **80** 3240
[7] Conti C, Peccianti M and Assanto G 2003 *Phys. Rev. Lett.* **91** 073901
[8] Mahan G D and Claro F 1988 *Phys. Rev. B* **38** 1963
[9] Hua C and Lindsay L 2020 *Phys. Rev. B* **102** 104310
[10] Bychenkov V Y, Rozmus W, Tikhonchuk V T and Brantov A V 1995 *Phys. Rev. Lett.* **75** 4405
[11] Baranov M A 2008 *Phys. Rep.* **464** 71
[12] Gallagher T F 1994 *Rydberg Atoms* (Cambridge: Cambridge University Press)
[13] Fleischhauer M, Imamoglu A and Marangos J P 2005 *Rev. Mod. Phys.* **77** 633
[14] Mohapatra A K, Jackson T R and Adams C S 2007 *Phys. Rev. Lett.* **98** 113003
[15] Wu Y Y, He Y H, Jiao Y C and Zhao J M 2024 *Chin. Phys. B* **33** 113201
[16] Peyronel T, Firstenberg O, Liang Q, Hofferberth S, Gorshkov A V, Pohl T, Lukin M D and Vuletić V 2012 *Nature* **488** 57
[17] Sevincli S, Henkel N, Ates C and Pohl T 2011 *Phys. Rev. Lett.* **107** 153001
[18] Pritchard J D, Weatherill K J and Adams C S 2013 *Annu. Rev. Cold At. Mol.* **1** 301
[19] Gorshkov A V, Nath R and Pohl T 2013 *Phys. Rev. Lett.* **110** 153601
[20] Firstenberg O, Adams C S and Hofferberth S 2016 *J. Phys. B* **49** 152003
[21] Bai Z and Huang G 2016 *Opt. Express* **24** 4442
[22] Murray C and Pohl T 2016 *Advances in Atomic, Molecular, and Optical Physics* (New York: Academic Press) **65** pp. 321–372
[23] Bai Z, Li W and Huang G 2019 *Optica* **6** 309
[24] Bai Z, Adams C S, Huang G and Li W 2020 *Phys. Rev. Lett.* **125** 263605

[25] Saffman M, Walker T G and Mølmer K 2010 *Rev. Mod. Phys.* **82** 2313
[26] Murray C and Pohl T 2017 *Phys. Rev. X* **7** 031007
[27] Jing M Y, Hu Y, Ma J, Zhang H, Zhang L J, Xiao L T and Jia S T 2020 *Nat. Phys.* **16** 911
[28] Ding D S, Liu Z K, Shi B S, Guo G C, Mølmer K and Adams C S 2022 *Nat. Phys.* **18** 1447
[29] Carr C, Tanasittikosol M, Sargsyan A, Sarkisyan D, Adams C S and Weatherill K J 2012 *Opt. Lett.* **37** 3858
[30] Gao Y, Ren Y, Yu D and Qian J 2019 *Phys. Rev. A* **100** 033823
[31] Bai Z Y, Zhang Q and Huang G X 2020 *Phys. Rev. A* **101** 053845
[32] Miroshnichenko A E, Flach S and Kivshar Y S 2010 *Rev. Mod. Phys.* **82** 2257